Supplementary information

Structural and metamorphic architecture of the Zanskar Himalaya, Suru Valley region, NW India: Implications for the evolution of the Himalayan metamorphic core

I.P. Cawood[1], M.R. St-Onge[1,2], O.M. Weller[3], M.P. Searle[1,4,5], D.J. Waters[1,4], T. Ahmad[6]

1. Department of Earth Sciences, University of Oxford, 3 South Parks Road, Oxford, OX1 3AN, UK.

2. Geological Survey of Canada, 601 Booth Street, Ottawa, Ontario, K1A 0E8, Canada.

3. Department of Earth Sciences, University of Cambridge, Downing Street, Cambridge, CB2 3EQ, UK.

4. Museum of Natural History, University of Oxford, Parks Road, Oxford, OX1 3PW, UK.

5. Camborne School of Mines, University of Exeter (Cornwall campus), Penryn, Cornwall, TR10 9EZ, UK.

6. Wadia Institute of Himalayan Geology, Dehradun 248 001, India.

Methods

The Zanskar Himalaya lies along the NW limit of the Indian monsoon system, resulting in reduced vegetation cover when compared to the central and eastern Himalaya. In addition, river gorges are deeply incised and provide up to *ca.* 3500 m of topographic relief between valley floor and surrounding peaks. Consequently, the study area is exceptionally well exposed.

Geological mapping was completed on 1:50,000 Sentinel-2 aerial imagery (Sentinel-2 L1C; September 2017, and August 2018) from Copernicus Open Access Hub (https://scihub.copernicus.eu/dhus/) and 100 m contours were produced in ArcMap (ArcGIS versions 10.5 to 10.7) using SRTM digital elevation data (SRTM 1-Arc second: September 2014) from USGS (https://earthexplorer.usgs.gov/). The basemap was produced using the WGS84 UTM zone 43N coordinate system. A GPS was used to reference the position (WGS84-UTM) of all outcrops, samples and measured structures in the field. Collected data and scanned field maps were georeferenced in ArcMap under the same coordinate system. The final geological map (Fig. 3) was compiled at 1:50,000 scale in Adobe Illustrator using a Sentinel-2 aerial imagery underlay (Sentinel-2 L1C; September 2021) from Copernicus Open Access Hub that was desaturated and exported from ArcMap to use as a universal basemap for all layers. All georeferenced data, maps and 200 m contours were exported from ArcMap and aligned to the aerial imagery underlay.

The geological map is constrained by field mapping (1,500 km^2) and remote-sensed mapping (900 km^2). The limit of field mapping is shown by the white dashed line in Figure 3. Remote-sensed mapping, outside this boundary was completed using data sources from Google Earth (version 7.3.4.8642; July 2013, October 2017, October 2019) and Copernicus Sentinel Hub (Sentinel-2 L1C; bands 4,3,2 and 12,4,2; September 2019, September 2021; https://apps.sentinel-hub.com/sentinel-playground/). No fold structures or isograds were extended through these regions. The remote-sensed data was also used in the field area to aid mapping or extend lithostratigraphic contacts, as well as structural features between traverses. Due to the range of elevation in the Suru Valley region, which varies from *ca.* 2,900 m around Sankoo to 7,135 m at the highest point at Nun, some fold structures in the field mapped area are inferred from exposures across mountain sides and from aerial imagery sources where the geology was inaccessible. These folds are annotated with an asterisk on Figure 3.

Primary bedding (S_0) was identified in rocks at low metamorphic grade (based on compositional layering) and subsequent deformation fabrics were characterized with respect to episodes of folding, shearing and/or transposition of the compositional anisotropy in sedimentary rocks. Porphyroblast growth-fabric development relationships, fabric defining metamorphic mineral assemblages, and shear sense were also used to distinguish differing fabrics. Index minerals in pelitic bulk compositions were used to map out the position of Barrovian metamorphic isograds, defined by chlorite- to sillimanite+K-feldspar-zone assemblages. Assemblages were also documented in metabasic units yielding a complementary sequence in actinolite (± tremolite) to hornblende+garnet zones. Where pelitic bulk compositions were absent in the metasedimentary rock sequence, assemblages from metavolcanic rocks were used to help constrain the equivalent metamorphic grades in pelitic compositions, with consequent uncertainties displayed on relevant

sections of the isograd linework of Figure 3.

Four cross sections (A-A', B-B', C-C', and D-D'; Fig. 4) were constructed to provide 3D constraints on the distribution of lithostratigraphic units and principal deformation features at depth and section lines were oriented sub-perpendicular to the orientation of the dominant regional fabric. In sections A-A' and D-D', the line of section is segmented to remain sub-perpendicular to major units and optimize proximity to field structural measurements. Apparent dips were calculated from structural measurements that were within approximately 3 km of a line of section and shown directly below topography on the associated cross section. Lithological contacts, isograds, and major faults and folds are extended 1,500 m above and below topography on the cross sections to better correlate between sections and deconvolve complicated regional structures. Across large portions of the map and cross sections folded strata are distinguished, rather than thrust imbricated sequences, based on consistent preservation of fold closures at mesoscale and macroscale; and evident lack of developed ductile mylonitic fabrics or brittle faults within the rock sequence (outside those marked on Figs 3 and 4).

Representative rock samples were collected at all metamorphic grades, and where possible were oriented relative to linear structural features in the field. When relevant, thin sections were cut parallel to the mineral stretching lineation and perpendicular to compositional layering to characterize shear sense.

Stereonets were generated for six different map transects (Fig. 8) using OpenStereo software (v2.0b Grohmann & Campanha, 2010). Contouring was applied in areas of sufficient data for stretching lineations or poles of foliation. A 1% area method for contours was applied using the estimation method of Robin & Jowett (1986). The Bingham method (Bingham, 1974) was used for mean vectors, mean planes, and mean fold axes as appropriate.

Lithostratigraphy

Indus Suture Zone

Dras Volcanics

The southern extent of the Dras Arc Complex is exposed in the Suru Valley. In the mapped region, the Dras Arc Complex outcrops as the Dras Volcanics, composing extrusive volcanic rocks (basalt and basaltic andesite) and epiclastic breccia. As only a minor component of the Dras Arc Complex is contained in the mapped region, additional details from previous studies in the region are brought in where relevant to lithological descriptions.

Extrusive volcanic rocks occur as dark green to pale green, locally layered, porphyritic to locally aphanitic lava flows (Fig. 5a). Porphyritic lava is dominated by clinopyroxene, hornblende and occasionally plagioclase-phyric basalt and basaltic andesite. Most clinopyroxene and hornblende range from mm-scale to $\leq$ 2 cm in length. Extrusive volcanic rocks are intercalated with subordinate volcaniclastic sandstone. Flows are several meters in thickness. Other studies from the region report the following: clinopyroxene is up to 10 cm in length (Searle, 1983); flows may range up to tens of meters in thickness (Honegger *et al.*, 1982; Robertson & Degnan, 1994);

pillow lavas are reported in certain layers at the base of the Dras Arc Complex (Juteau & Reibel, 1981; Searle, 1983; Robertson & Degnan, 1994). Further to the north the Dras Volcanics also include minor andesite and dacite (Fuchs, 1982; Honegger *et al.*, 1982; Searle, 1983).

Epiclastic breccia outcrops as massive, poorly sorted and weakly stratified bodies that are light grey to pale brown in color and locally light green to maroon (Fig. 5b). It is composed of heterogenous mm- to 10s of cm-scale sub-angular to sub-rounded clasts of volcanic extrusive units, dolerite, gabbro, red radiolarian chert and carbonates within a volcaniclastic to tuffaceous matrix. This unit is best exposed S of Dras at the contact to the underlying Lamayuru Complex. Up to meter-sized clasts are reported from other studies in the region and the thickness of these successions range up to hundreds of meters thick and occur interlayered with lavas (Searle, 1983; Robertson & Degnan, 1994).

Detailed descriptions of the Dras Volcanics and the greater Dras Arc Complex, including the lithologies found outside the mapped region are given in Honegger *et al.* (1982), Searle (1983), Robertson & Degnan (1994), Reuber *et al.* (1989), Bhat *et al.* (2019), Walsh *et al.* (2019). Metamorphism of the Dras Volcanics ranges from zeolite to lower greenschist facies. Ages of the Dras Arc range from 160 ± 3 Ma to 80 ± 1 Ma in Walsh *et al.* (U-Pb zircon; 2019), with the younger pulse also reported by older studies at *ca.* 82–70 Ma ($^{40}Ar/^{39}Ar$ Hornblende, K-Ar white mica and biotite; Brookfield & Reynolds, 1981; Honegger *et al.*, 1982).

Lamayuru Complex - Metasedimentary units

Graphitic pelite is dark grey to black, fine-grained and finely laminated with a prominent cleavage (Fig. 5c). The unit weathers easily and defines most of the scree slopes within the zones west and east from Sankoo. The unit has a structural thickness of $\sim$ 2–4 km. Locally, thin 1-10 cm thick horizons of metamarl or metacarbonate are interlayered with the graphitic pelite. The unit is dominated by graphitic phyllite, with zones locally containing mm-scale biotite and albite porphyroblasts at the relevant metamorphic grade.

The graphitic pelite grades into a mixed pelite, psammite, and semipelite. It is light grey to pale green, fine- to medium-grained and appears layered to finely laminated (Fig. 5d). The transition zone shows thicker mm- to cm-scale graphite-rich layers of psammite or semipelite with thin mm-scale laminae of pelite and fining upwards grading. The unit is best characterised by alternating layers of approximately equal thickness of pelite with psammite and or semipelite. This lowermost structural zone contains mm-scale porphyroblastic titanite in pelite layers, and/or ankerite or calcite in psammite layers. This unit has a maximum structural thickness of $\sim$ 1.5 km and is dominated by chlorite biotite schist.

The lithostratigraphically highest unit of the Lamayuru Complex as exposed in the Suru Valley area is a mixed graphitic pelite, semipelite and metacarbonate. The contact from the underlying mixed pelite, psammite, and semipelite is gradational. The mixed graphitic pelite, semipelite, and metacarbonate is dark grey, fine-grained, and finely laminated (Fig. 5e). Cm-scale horizons of metamarl and metacarbonate are repeated throughout. The unit has a maximum structural thickness of approximately 200 m and comprises graphitic calc-phyllite and

calc-schist.

Lamayuru Complex - Metavolcanic rocks

Group B metavolcanic rocks are light to dark green, fine-grained and have a layered appearance when metamorphosed to greenschist facies and massive, blocky appearance with mm-scale quartz veins where in the sub-greenschist facies N of Umba (Fig. 3, 5f). The quartz veins have a lenticular shape in outcrop and/or occur as discontinuous layers within the graphitic pelite. Green to dark grey graphitic phyllites and locally cm-thick metacarbonates (within the graphitic pelite unit) are often intercalated with the group B metavolcanic rocks at cm- to m-scale. These rocks comprise actinolite schist, and meta-alkali basalt or meta-alkali andesite.

Greater Himalayan Sequence and Tethyan Himalayan Sequence

Metasedimentary units

The lithostratigraphically (and structurally) lowest level of the Greater Himalayan Sequence–Tethyan Himalayan Sequence is dark-colored, medium-grained, and finely laminated pelite (Figure 5g). The true structural thickness of the pelite unit is unknown thought displays a maximum across strike extent of $\sim$ 4 km. The unit is dominated by kyanite-staurolite schist with a porphyroblastic texture.

The pelite unit grades upwards into a mixed package of psammite, pelite and semipelite. Psammite is the most abundant component and appears relatively homogenous to thickly layered in outcrop. It is light grey, fine- to medium-grained and displays fining upwards grading (Figure 5h). Pelite and semipelite layers are dark colored, medium-grained, locally graphite- and carbonate mineral-rich and are characterized by thin laminae capping the psammite or as individual layers. The mixed psammite, pelite and semipelite has the largest structural thickness in the study area (km-scale) and is present at all metamorphic grades. In outcrop, the unit can be described as a schist or gneiss with associated porphyroblasts of the relevant metamorphic grade.

At or near the top of the mixed pelite, semipelite and psammite sequence, is a locally developed light grey, fine-grained and equigranular psammite (Fig. 5i). The unit appears homogenous to layered in outcrop. The thickness of the unit is generally $<$ 100 m. Composition ranges from arkosic to quartzitic. 1–2 mm garnets are often present, but index minerals of higher metamorphic grades are not.

Metacarbonate outcrops within 1 km of the equigranular psammite and locally overlies the unit. It is cream to light grey and fine- to medium-grained with a granoblastic texture (Figure 5j). In outcrop it is layered to homogenous and varies from thinly to thickly bedded (m-scale to 200 m) and is as a marble.

The uppermost lithostratigraphic unit of the Greater Himalayan Sequence–Tethyan Himalayan Sequence in the Suru Valley comprises a mixed package of semipelite, metacarbonate, and pelite. The semipelite and pelite are dark grey to black and are fine- to medium-grained (Figure 5k). They are finely laminated to layered and locally show a dominant graphitic and

carbonaceous component. The metacarbonate is light grey with characteristic orange weathering and fine-grained with a granoblastic texture. Metacarbonate often alternates and/or is folded into the semipelite and pelite such that it alternates at cm-scale and locally at 10–100 m-scales. The mixed semipelite, metacarbonate and pelite dominantly outcrops at the edges of the mapped area (Fig. 3) and is occasionally folded into the mixed psammite, pelite, and semipelite. The mixed semipelite, metacarbonate and pelite shows variation in mineral assemblage, grain size and color across the mapped area though generally is as a calc-schist.

Metavolcanic and subvolcanic rocks

Group A comprises dark green, fine- to medium-grained metamorphosed subvolcanic and volcanic rocks and are layered at mm- to cm-scale (Figure 5l). The group generally occurs as discontinuous sheets within the mixed semipelite, metacarbonate and pelite, and/or defining the contact between this mixed unit and the mixed psammite, pelite, and semipelite (Fig. 3). In outcrop, group A metamorphosed volcanic rocks vary in unit thickness from cm-scale to 250 m). These rocks are amphibolite. Geochemical studies (Sr-Nd isotopes; whole rock major and trace elements) suggest these units are the metamorphosed equivalents of the lower Pemian Panjal Trap volcanics (Honegger *et al.*, 1982; Shellnutt, 2018). The Panjal Trap volcanics (Lydekker, 1883; Wadia, 1961) are known to be aphyric tholeiitic to mildly alkalic in composition (Shellnutt, 2018). They represent basalt flow covering an area of approximately 12,000 km^2 that mark the end of volcanic activity that began in the late Carboniferous and record the break-up of Gondwana (Pareek, 1976; Honegger *et al.*, 1982; Shellnutt, 2018).

Metamorphosed granites

Three types of metamorphosed granite occur in the Suru Valley, which from oldest to youngest are biotite-muscovite syenogranite, garnet-biotite-muscovite granite and garnet tourmaline leucogranite (Fig. 5m–o). The garnet tourmaline leucogranite is present as < 40 m bodies within the mapped area, therefore are only locally recorded on Figures 3 and 4. The leucogranites become more extensive S of the Suru Valley region (Fig. 2), and are associated with the sillimanite-grade migmatites in the highest-grade zone of the Himalayan metamorphic core (Searle, 1986).

The biotite-muscovite syenogranite is light grey to cream, coarse-grained and frequently porphyritic, containing coarse poikiloblastic K-feldspar phenocrysts (1–10 cm; Fig. 5m). In regions of lower strain, the granite possesses a coarse equigranular texture. In proximity to shear zones, the granite displays increased evidence of deformation and shows an augen gneiss texture (comprising K-feldspar) with a prominent C-S-C' fabric. At the regional scale, syenogranite form km-scale bodies that are sub-parallel to the regional tectonic foliation.

The garnet-biotite-muscovite granite is light grey to cream, medium- to coarse-grained and outcrops as homogeneous sill-like bodies parallel or sub-parallel to the regional tectonic fabric (Figs. 3 and 5n). These bodies vary from monzogranite (e.g., S of Sankoo; Fig. 5n) to syenogranite (e.g., Shafat) in composition, the latter are frequently porphyritic, containing coarse poikiloblastic K-feldspar phenocrysts (0.5–6 cm). A medium-grained more leucocratic

phase of the granite is commonly emplaced subparallel to the fabric in the granite. The leucocratic phase of the granite exhibits more mafic-rich rims in contact to the adjacent units. Fine-grained, and pegmatitic leucocratic phases were also identified. Field relations do not infer consistent crosscutting relationships and therefore differing ages between the different phases (though the fine-grained, and pegmatitic leucocratic phases generally crosscut the fabric in the granite). As such, the different phases and compositions (monzogranite, syenogranite, minor leucocratic phases) are interpreted to represent intrusive components of a single granitic complex. In outcrop, large bodies of granite are associated with group A metavolcanic rocks. The group A metavolcanic rocks (generally $\leq$1.5 m thickness) appear to have intruded as sills into the granite as observed at the Sankoo granite (Fig. 3), as has been previously suggested (Walker, 1999; Noble *et al.*, 2001). However, field relations also indicate that the group A metavolcanic rocks may also appear as xenoliths within the granite. At the regional scale, the granite forms km-scale bodies or layers that are parallel to the regional tectonic foliation, though some discordance between intrusive contacts and deformation fabrics in the host rocks is visible in outcrop (e.g., Shafat). Dating of the garnet-biotite-muscovite granite at Sankoo has yielded a Permian age of 268 $\pm$ 5 Ma, and discordant results at Parkachik suggests an age of *ca.* 270 Ma (U-Pb zircon; Noble *et al.*, 2001). Another outcrop of the granite at Tongul has also been dated at 284 $\pm$ 4.4 Ma (U-Pb zircon Horton & Leech, 2013).

The garnet tourmaline leucogranite is white to cream colored, fine- to coarse-grained leucogranite with an irregular to lenticular shape in outcrop (Fig. 5o). Layers of garnet tourmaline leucogranite define a stromatitic layering in the metasedimentary sequence, both subparallel and discordant to the regional fabric. Coarse cm-scale tourmaline is present locally. Where leucogranite is coarse grained it occurs as pegmatite. Pegmatite forms tabular to lenticular bodies and may crosscut or lie parallel to dominant regional foliation. U-Pb monazite dating of leucogranites from Zanskar give an age of *ca.* 20.8–19.5 Ma for crustal melting, with those dated at Shafat producing a measured age of 20.8 $\pm$ 0.3 Ma (Noble & Searle, 1995).

Migmatite

Although migmatite is not shown on the geological map in Figure 3, it is present just SSW of Rangdum in the Lalung valley (Fig. 2). Migmatite is characterized by white–cream, medium-grained, wavy to lenticular leucosome (Fig. 5p). The leucosome occurs as cm to 10s of cm long discontinous lenses that lie sub-parallel and/or crosscut the dominant regional foliation. Boundaries between the leucosome and the neosome are curvilinear to interlobate and are often defined by increased mica and aluminosilicate content (interpreted as residuum). The mixed psammite, pelite, and semipelite unit is inferred to comprise the paleosome, with most of the melting occurring in the fertile pelitic layers. These textures are consistent with *in situ* migmatisation and are absent within leucogranite which is therefore interpreted to represent structurally higher coalesced products of *in situ* partial melting. This is supported by the U-Pb monazite ages of leucogranite from Noble & Searle (1995) which overlap with ages for migmatites (Figure S2).

Fabric defining metamorphic mineral assemblages

$S_0/S_1/L_1$

The oldest deformation fabric (S_1) identified in the study area is defined in metasedimentary rocks by the alignment of phyllosilicate minerals (chlorite, muscovite, and biotite) and flattening of quartz and feldspar. In metavolcanic rocks, S_1 is defined by preferred orientation of chlorite, biotite and locally by mats of actinolite and tremolite and albite-quartz laminations. S_1 is associated with a well-developed NE-plunging lineation (L_1), defined in metasedimentary rock by elongate rods of quartz and feldspar and alignment of phyllosilicate minerals. In metavolcanic rocks, L_1 is defined by the orientation of actinolite and tremolite and the alignment of chlorite and biotite.

$S_2/L_2/F_2$

S_2 is defined in metasedimentary rocks by the growth of muscovite and biotite along cleavage domains and the segregation of quartz and feldspar into microlithons. Where the fabric is penetrative it is defined by a strong layering of muscovite and biotite and flattened grains of quartz and feldspar. In metavolcanic rocks S_2 is defined by the preferred orientation of chlorite, biotite, plagioclase-quartz laminations, and mats of tremolite, actinolite, and/or hornblende. L_2 is defined in metasedimentary rocks by the alignment of muscovite and biotite, and quartz and feldspar rods and in metavolcanic rocks by the orientation of tremolite, actinolite, and/or hornblende, and alignment of chlorite, and/or biotite.

$S_3/L_3/F_3$

S_3 is defined in metasedimentary rocks by the alignment of biotite, muscovite, and/or chlorite. Growth of biotite and retrogressive chlorite is also observed along shear bands. In metavolcanic rocks, S_3 is defined by a preferred orientation of biotite and/or chlorite, mats of hornblende, actinolite and/or tremolite, and plagioclase-quartz. L_3 is characterized by alignment of phyllosilicate minerals and rods of quartz and feldspar in metasedimentary rocks. In metavolcanic rocks L_3 is defined by the orientation of hornblende, actinolite and alignment of biotite and chlorite.

Further relationship of metamorphic minerals to penetrative fabrics

These additional phases detail the relationship of prograde–peak metamorphism relative to fabric development.

Biotite within metavolcanic rocks appears aligned with S_2, although biotite porphyroblasts also show evidence of overgrowing the same fabric. This suggests syn- to post-D_2 growth of biotite as reported for the metasedimentary rocks.

Ilmenite and rutile within the metasedimentary and metavolcanic sequence often appears aligned with S_2. Examples of rutile overgrowing the S_2 fabric are documented within the

metasedimentary rock sequence. Where ilmenite is present as S_2 inclusions in garnet it is disjunctive with the matrix S_3 fabric. These observations imply syn-D_2 and pre-D_3 growth of ilmenite and syn- to post-D_2 growth of rutile.

Titanite within the graphitic mixed semipelite, psammite, and pelite overgrows the S_2 fabric and is aligned to crenulations formed by D_3. This suggests post-D_2 growth of titanite within this sequence.

Supplementary Figures

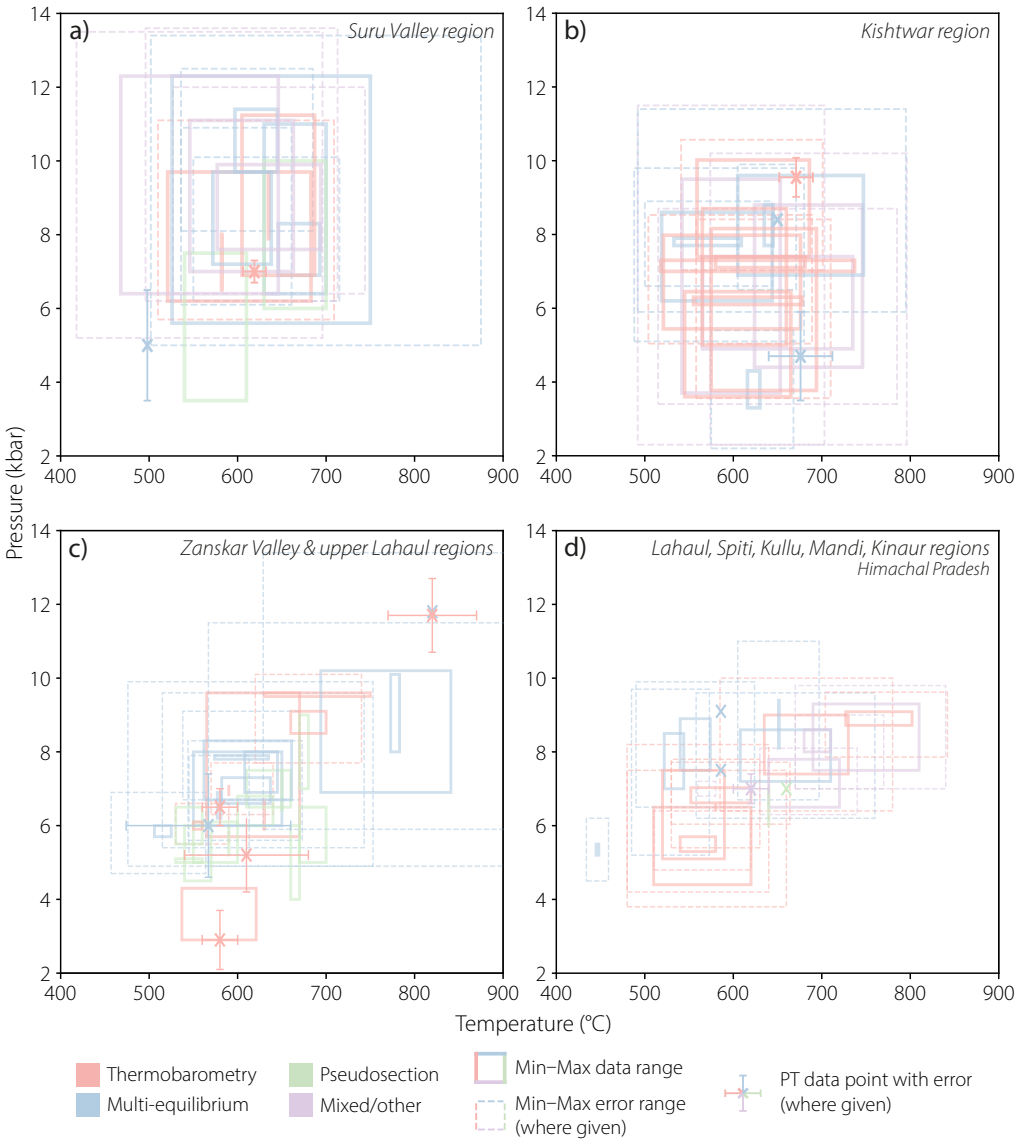

Figure S1: Summary of published P-T data for the Himalayan metamorphic core of the a) Suru Valley region, b) Kishtwar region, c) Zanskar Valley and upper Lahaul regions, and d) Lahaul, Spiti, Kullu, Mandi, Kinaur regions in Himachal Pradesh (see Fig. 2). Due to debated trend of the South Tibetan Detachment System and correlation of units in the Himachal Pradesh (e.g., Stübner *et al.*, 2014), P-T data includes areas above and below the South Tibetan Detachment where defined, thereby locally comprising units assigned to greenschist- to amphibolite-facies units of the THS (e.g., Chambers *et al.*, 2009). Core compositions used in thermobarometry are generally excluded with the exception of results from Stephenson (1997), Stephenson *et al.* (2000) or where inferred to correlate to peak. Suru Valley region P-T data: Gilbert (1986), Searle *et al.* (1992), Vance *et al.* (1998), Walker (1999), Searle *et al.* (1999), Walker *et al.* (2001); Kishtwar region P-T data: Stäubli (1988, 1989), Guntli (1993), Jain & Manickavasagam (1993), Stephenson (1997), Manickavasagam *et al.* (1999), Searle *et al.* (1999), Stephenson *et al.* (2000); Zanskar Valley and upper Lahaul regions: Jain & Manickavasagam (1993), Dransfield (1994), Pognante & Lombardo (1989), Pognante *et al.* (1990), Pognante (1992), Dèzes *et al.* (1999), Manickavasagam *et al.* (1999), Walker *et al.* (1999), Robyr (2002), Finch *et al.* (2014), Štípská *et al.* (2020); Lahaul, Spiti, Kullu, Mandi, Kinnaur regions (Himachal Pradesh): Stephenson (1997), Vannay & Grasemann (1998), Manickavasagam *et al.* (1999), Vannay *et al.* (1999), Wyss (2000), Thakur & Tripathi (2008), Chambers *et al.* (2009), Leger *et al.* (2013).

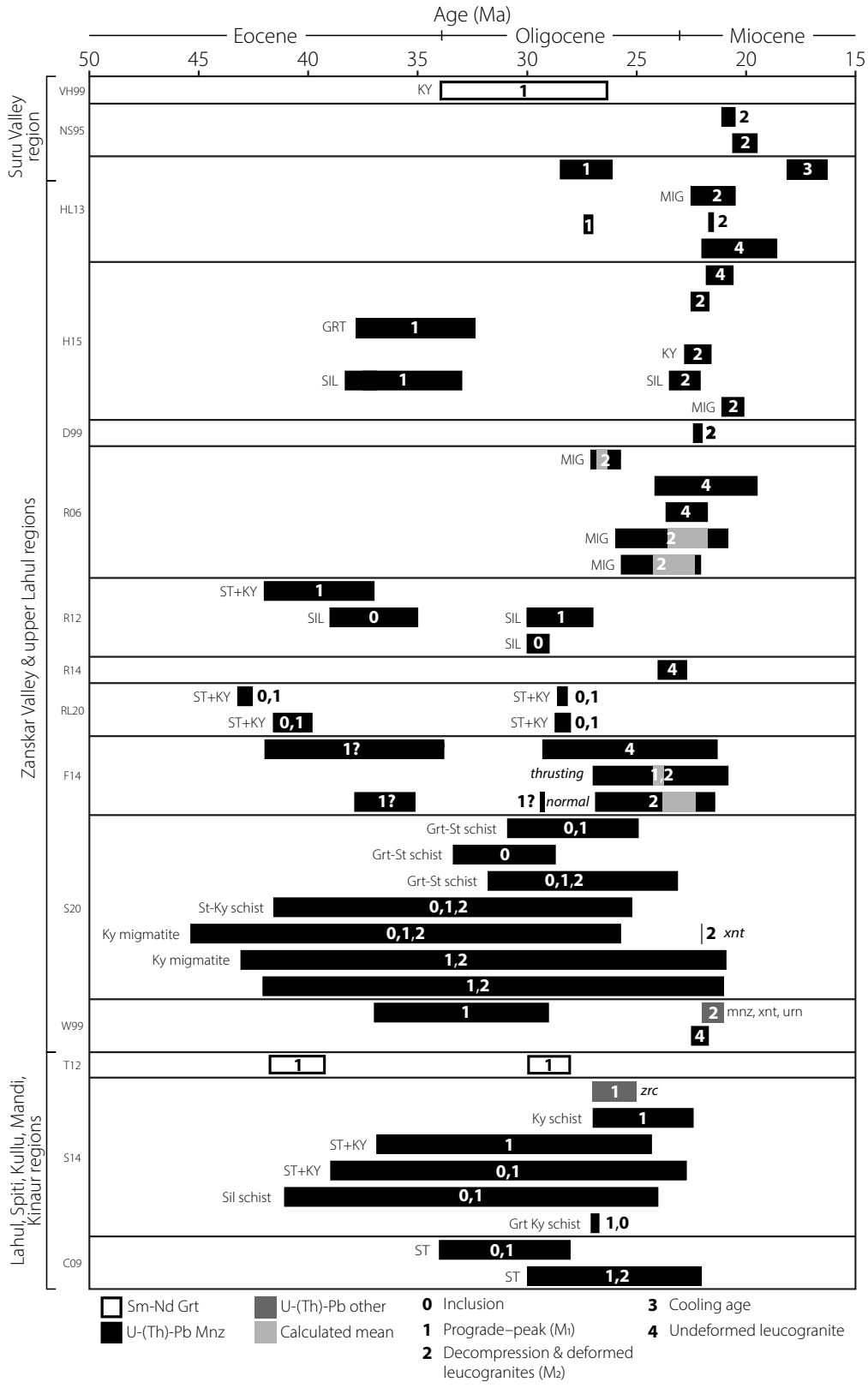

Figure S2: Summary of published geochronological data for Himalayan metamorphic core rocks of the Suru Valley, Zanskar Valley, and Himachal Pradesh. Ranges include reported error. VH99 — Vance & Harris (1999), NS95 — Noble & Searle (1995), HL13 — Horton & Leech (2013), H15 — Horton *et al.* (2015), D99 — Dèzes *et al.* (1999), R06 — Robyr *et al.* (2006), R12 — Robyr *et al.* (2012), R14 — Robyr *et al.* (2014), RL20 — Robyr & Lanari (2020), F14 — Finch *et al.* (2014), S20 — Štípská *et al.* (2020), W99 — Walker *et al.* (1999), T12 — Thöni *et al.* (2012), S14 — Stübner *et al.* (2014), C09 — Chambers *et al.* (2009).

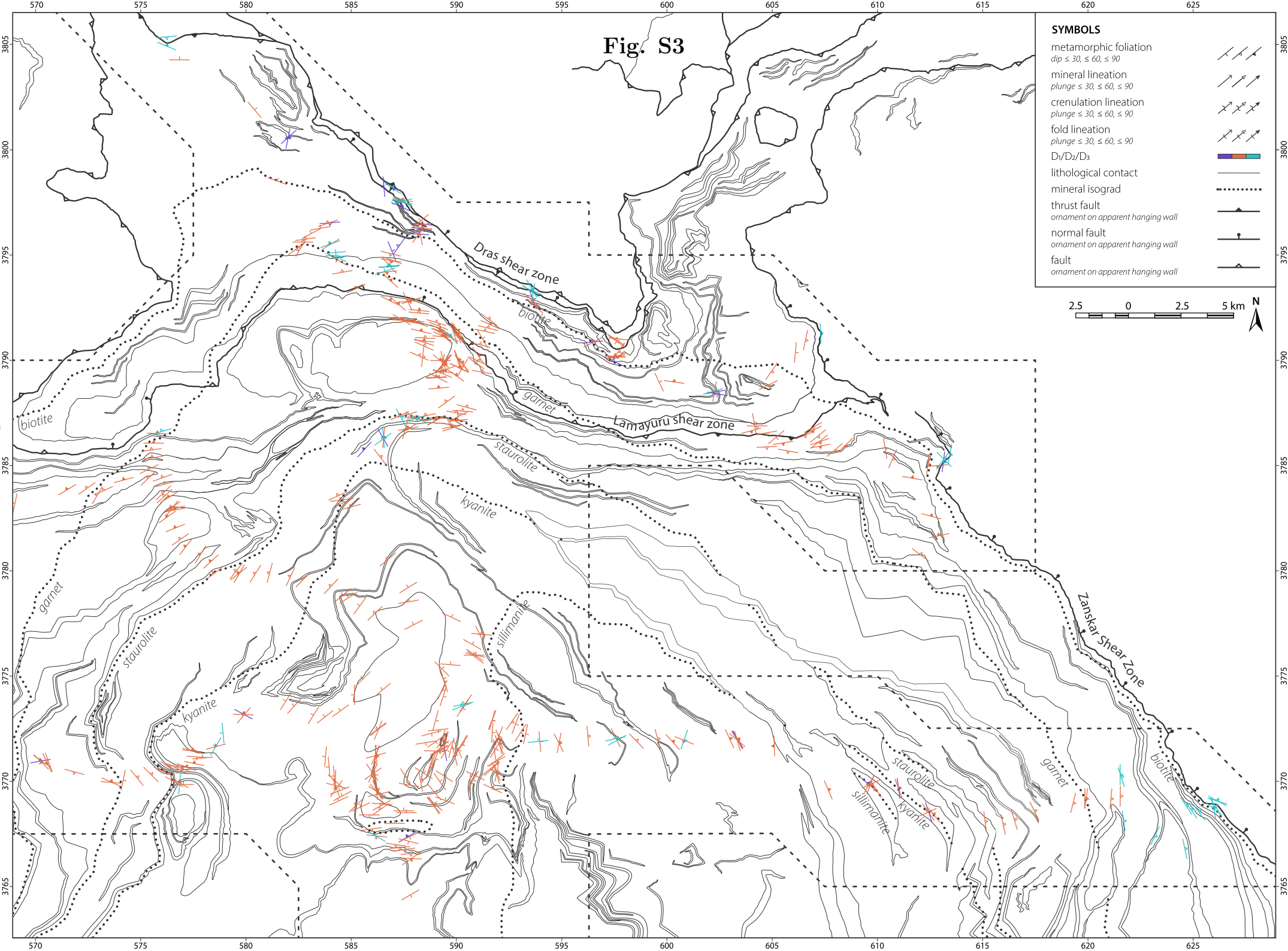
Fig. S3
SYMBOLS
metamorphic foliation
dip ≤ 30, ≤ 60, ≤ 90
mineral lineation
plunge ≤ 30, ≤ 60, ≤ 90
crenulation lineation
plunge ≤ 30, ≤ 60, ≤ 90
fold lineation
plunge ≤ 30, ≤ 60, ≤ 90
D1/D2/D3
lithological contact
mineral isograd
thrust fault
ornament on apparent hanging wall
normal fault
ornament on apparent hanging wall
fault
ornament on apparent hanging wall
2.5 0 2.5 5 km
N
Dras shear zone
Lamayuru shear zone
Zanskar Shear Zone
biotite
garnet
staurolite
kyanite
sillimanite
570
575
580
585
590
595
600
605
610
615
620
625
3805
3800
3795
3790
3785
3780
3775
3770
3765

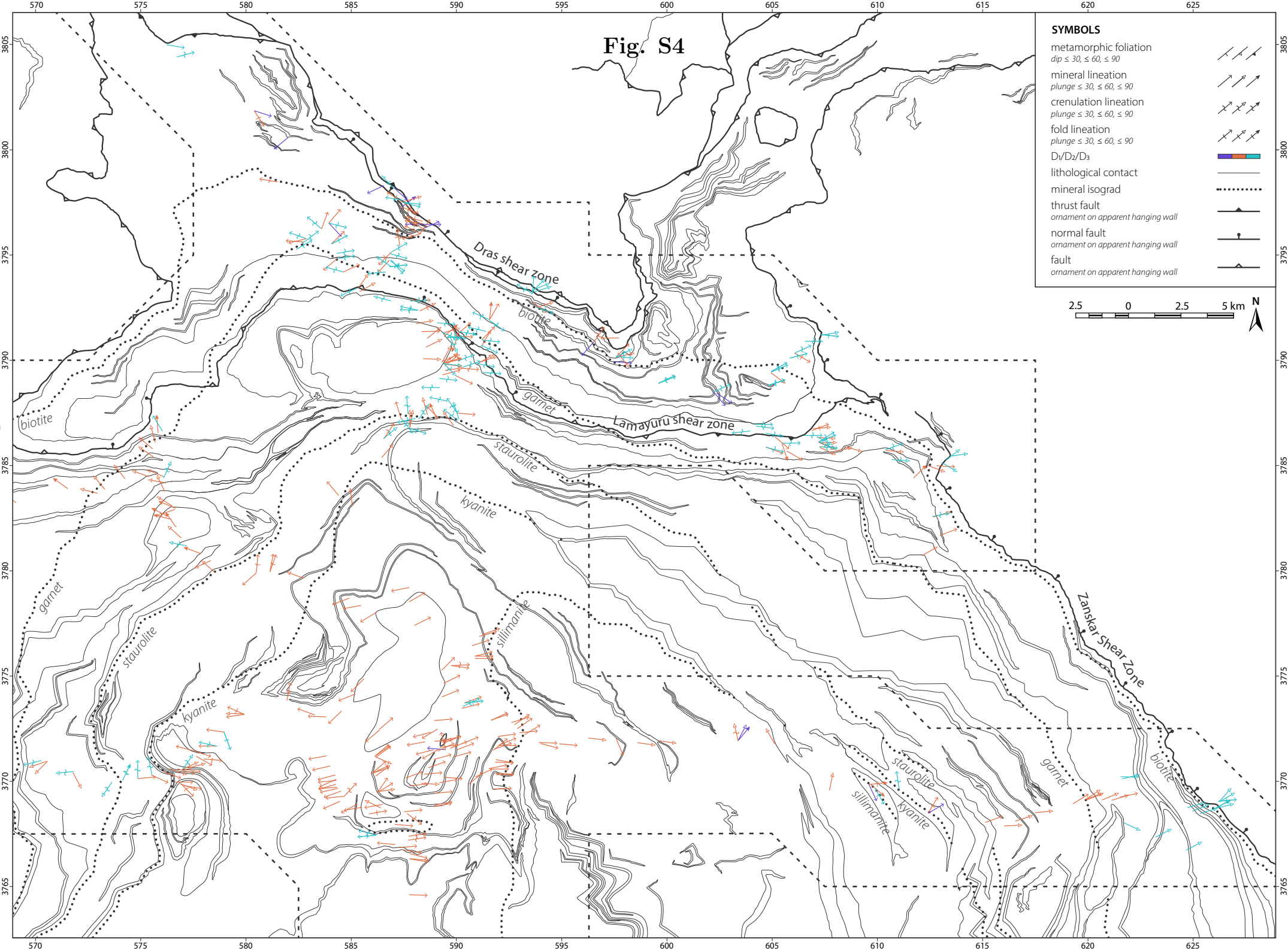
Fig. S4
SYMBOLS
metamorphic foliation
dip ≤ 30, ≤ 60, ≤ 90
mineral lineation
plunge ≤ 30, ≤ 60, ≤ 90
crenulation lineation
plunge ≤ 30, ≤ 60, ≤ 90
fold lineation
plunge ≤ 30, ≤ 60, ≤ 90
D1/D2/D3
lithological contact
mineral isograd
thrust fault
ornament on apparent hanging wall
normal fault
ornament on apparent hanging wall
fault
ornament on apparent hanging wall
2.5 0 2.5 5 km
N
Dras shear zone
Lamayuru shear zone
Zanskar Shear Zone
biotite
garnet
staurolite
kyanite
sillimanite
570
575
580
585
590
595
600
605
610
615
620
625
3805
3800
3795
3790
3785
3780
3775
3770
3765

Figure S3: Form-line map of major lithological, tectonic and metamorphic features of the Suru Valley area with planar structural elements colored by associated deformation event. Grid references are truncated, with final three zeros omitted.

Figure S4: Form-line map of major lithological, tectonic and metamorphic features of the Suru Valley area with linear structural elements colored by associated deformation event. Grid references are truncated, with final three zeros omitted.

Figure S5: Original panoramic field photographs of macroscale fold structures. Matching annotated panoramic photographs are found in Fig. 7. a) Oblique perspective of the Donara antiform at the river confluence along Chellong Nala, view to the N. b) intersecting folds above Parkachik glacier, view to the ESE. c) view above Tongul over to Parkachik metagranite and intersecting folds, view to the S.

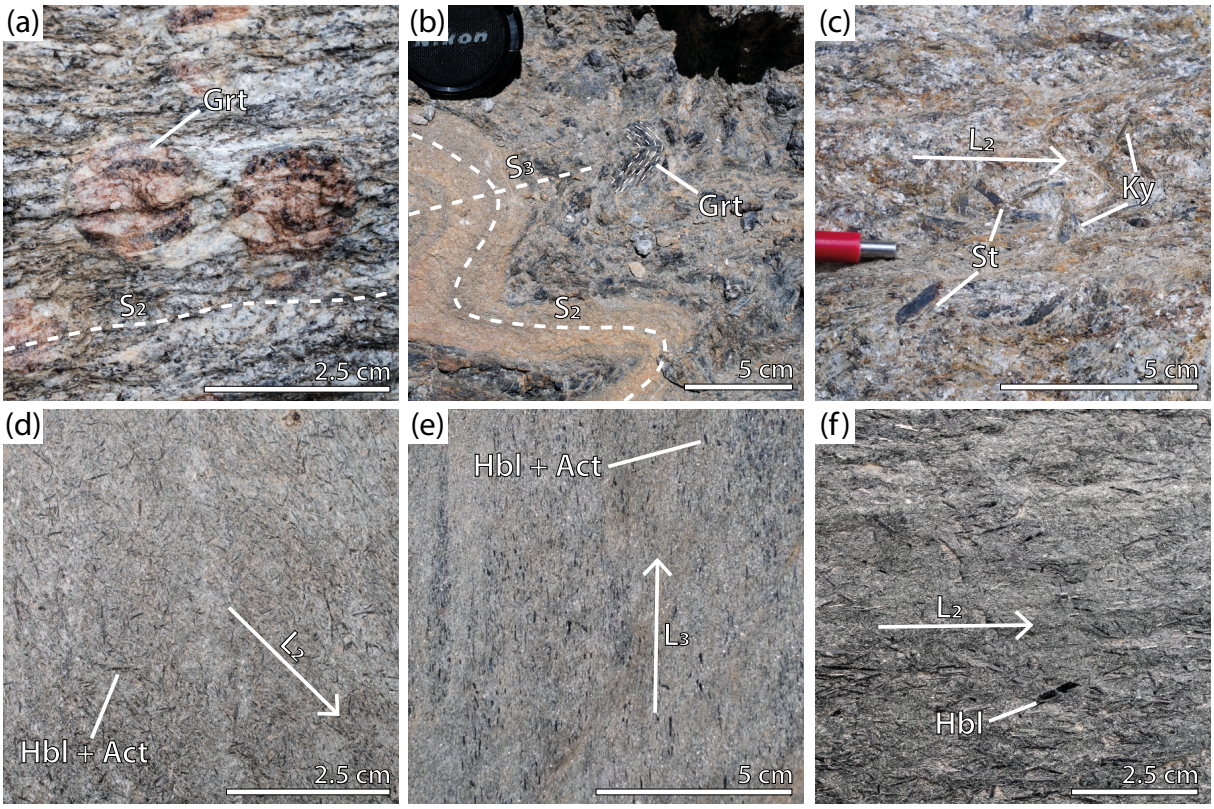

Figure S6: Mesoscale field photos of mineral growth relative to fabric development during D_{2-3}. a) Garnet porphyroblast overgrowing S_2 fabric, and in the core showing clockwise rotation synchronous with S_2. b) Mesoscale F_3 folds developing a crenulation cleavage of S_2, garnet shows inclusion trails suggesting growth after D_2 but prior to F_3 folding. c) Pelite with staurolite and kyanite porphyroblasts crosscutting the L_2 mineral stretching lineation. d) Group A metavolcanic rock showing actinolite and hornblende needles crosscutting L_2. e) Group A metavolcanic rock with actinolite and hornblende needles reoriented parallel to L_3. f) Group A metavolcanic rock showing tabular hornblende crystals both crosscutting and aligned relative to L_2.

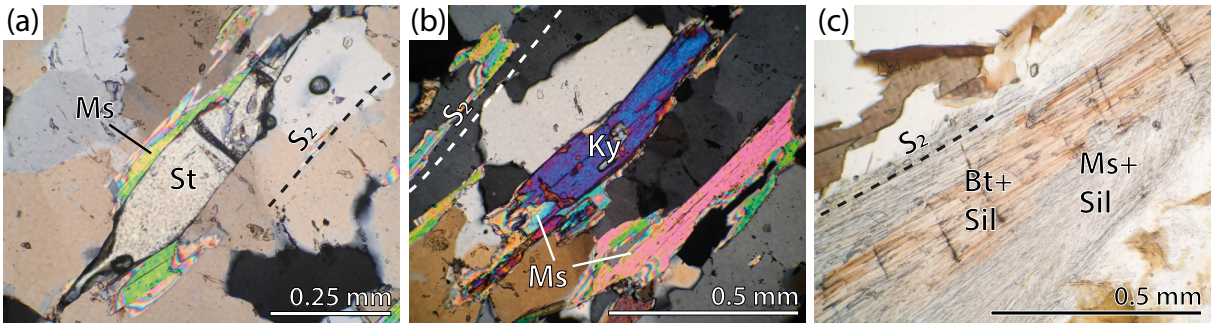

Figure S7: Shape preferred orientation of a) staurolite, and b) kyanite parallel to S_2 aligned micas, possibly nucleating mimetically on and overgrowing such phyllosilicates (dominantly muscovite). Epitaxial growth of c) fibrolitic sillimanite on biotite and muscovite. These observations suggest that all peak mineral growth at these grades demonstrably occured after the development of the S_2 fabric. Alternatively, staurolite and kyanite growth may have begun in select compositions during D_2.

References

Bhat, I. M., T. Ahmad, & D. V. S. Rao (2019), Petrology and Geochemistry of Mafic Intrusive Rocks from the Sapi-Shergol Ophiolitic Mélange, Indus Suture Zone, Western Ladakh: Constraints on Petrogenesis and Tectonic Setting, *The Journal of Geology*, 127(5), 543–566, doi:10.1086/704254.

Bingham, C. (1974), An Antipodally Symmetric Distribution on the Sphere, *The Annals of Statistics*, 2(6), 1201–1225.

Brookfield, M. E., & P. H. Reynolds (1981), Late Cretaceous emplacement of the Indus suture zone ophiolitic mélanges and an Eocene-Oligocene are on the northern edge of the Indian plate, *Earth and Planetary Science Letters*, 55, 157–162, doi:10.1016/0012-821X(81)90094-7.

Chambers, J., M. Caddick, T. Argles, M. Horstwood, S. Sherlock, N. Harris, R. Parrish, & T. Ahmad (2009), Empirical constraints on extrusion mechanisms from the upper margin of an exhumed high-grade orogenic core, Sutlej valley, NW India, *Tectonophysics*, 477(1-2), 77–92, doi:10.1016/J.TECTO.2008.10.013.

Dèzes, P. J., J. C. Vannay, A. Steck, F. Bussy, & M. Cosca (1999), Synorogenic extension: Quantitative constraints on the age and displacement of the Zanskar shear zone (northwest Himalaya), *GSA Bulletin*, 111(3), 364–374, doi:10.1130/0016-7606(1999)111⟨0364:SEQCOT⟩2.3.CO;2.

Dransfield, M. (1994), Extensional exhumation of high-grade metamorphic rocks in Western Norway and the Zanskar Himalaya, Ph.D. thesis, University of Oxford.

Finch, M., P. Hasalová, R. F. Weinberg, & C. M. Fanning (2014), Switch from thrusting to normal shearing in the Zanskar shear zone, NW Himalaya: Implications for channel flow, *GSA Bulletin*, 126(7-8), 892–924, doi:10.1130/B30817.1.

Fuchs, G. (1982), The geology of Western Zanskar, *Jahrbuch der Geologischen Bundesanstalt*, 125(1-2), 1–50.

Gilbert, E. (1986), Évolution structurale d'une chaine de collision : Structures et déformation dans le nord de la plaque indienne en Himalaya du Ladakh (cristallin du haut Himalaya et séries téthysiennes), These de doctorat, Poitiers.

Grohmann, C. H., & G. A. C. Campanha (2010), OpenStereo: Open Source, Cross-Platform Software for Structural Geology Analysis, in AGU Fall Meeting, pp. IN31C–06, San Francisco, CA.

Guntli, P. (1993), Geologie und Tektonik des higher und Lesser Himalaya im Gebiet von Kishtwar, SE Kashmir (NW Indien), Doctoral Thesis, ETH Zurich.

Honegger, K., V. Dietrich, W. Frank, A. Gansser, M. Thöni, & V. Trommsdorff (1982), Magmatism and metamorphism in the Ladakh Himalayas (the Indus-Tsangpo suture zone), *Earth and Planetary Science Letters*, 60(2), 253–292, doi:10.1016/0012-821X(82)90007-3.

Horton, F., & M. L. Leech (2013), Age and origin of granites in the Karakoram shear zone and Greater Himalaya Sequence, NW India, *Lithosphere*, 5(3), 300–320, doi:10.1130/L213.1.

Horton, F., J. Lee, B. Hacker, M. Bowman-Kamaha'o, & M. Cosca (2015), Himalayan gneiss dome formation in the middle crust and exhumation by normal faulting: New geochronology of Gianbul dome, northwestern India, *Bulletin of the Geological Society of America*, 127(1-2), 162–180, doi:10.1130/B31005.1.

Jain, A. K., & R. M. Manickavasagam (1993), Inverted metamorphism in the intracontinental ductile shear zone during Himalayan collision tectonics, *Geology*, 21(5), 407–410, doi:10.1130/0091-7613(1993)021⟨0407:IMITID⟩2.3.CO;2.

Juteau, T., & G. Reibel (1981), Indus suture: Petrographic description of the pillow-lavas of the Dras formation, and of the ophiolites of the Spongtang-Photaksar nappe, in 1st Meeting EUG, p. 19, Terra Cognita Special Issue, Strasbourg.

Leger, R. M., A. A. G. Webb, D. J. Henry, J. A. Craig, & P. Dubey (2013), Metamorphic field gradients across the Himachal Himalaya, northwest India: Implications for the emplacement of the Himalayan crystalline core, *Tectonics*, 32(3), 540–557, doi:10.1002/tect.20020.

Lydekker, R. (1883), The geology of the Kashmir and Chamba territories and the British district of Khagan, *Mem. Geol. Surv. India*, 22, 31–34.

Manickavasagam, R., A. Jain, S. Singh, & A. Asokan (1999), Metamorphic evolution of the northwest Himalaya, India: Pressure-temperature data, inverted metamorphism, and exhumation in the Kashmir, Himachal, and Garhwal Himalayas, *Special Paper of the Geological Society of America*, 328, 179–198, doi:10.1130/0-8137-2328-0.179.

Noble, S. R., & M. P. Searle (1995), Age of crustal melting and leucogranite formation from U-Pb zircon and monazite dating in the western Himalaya, Zanskar, India, *Geology*, 23(12), 1135–1138, doi:10.1130/0091-7613(1995)023⟨1135:AOCMAL⟩2.3.CO;2.

Noble, S. R., M. P. Searle, & C. B. Walker (2001), Age and Tectonic Significance of Permian Granites in Western Zanskar, High Himalaya, *The Journal of Geology*, 109(1), 127–135, doi:10.1086/317966.

Pareek, H. S. (1976), On studies of the agglomeratic slate and Panjal Trap in the Jhelum, Liddar and Sind Valleys, Kashmir, *Rec. Geol. Surv. India*, 107/2, 12–37.

Pognante, U. (1992), Migmatites and Leucogranites of tertiary age from the high Himalayan Crystallines of Zanskar (NW India): A case history of anatexis of Palaeozoic orthogneisses, *Mineralogy and Petrology*, 46(4), 291–313, doi:10.1007/BF01173569.

Pognante, U., & B. Lombardo (1989), Metamorphic evolution of the High Himalayan Crystallines in SE Zanskar, India, *Journal of Metamorphic Geology*, 7(1), 9–17, doi:10.1111/J.1525-1314.1989.TB00571.X.

Pognante, U., D. Castelli, P. Benna, G. Genovese, F. Oberli, M. Meier, & S. Tonarini (1990), The crystalline units of the High Himalayas in the Lahul-Zanskar region (northwest India):

Metamorphic-tectonic history and geochronology of the collided and imbricated Indian plate, *Geological Magazine*, 127(2), 101–116, doi:10.1017/S0016756800013807.

Reuber, I., R. Montigny, & R. Thuizat (1989), K-Ar ages of ophiolites and arc volcanics of the Indus suture zone : Clues on the early evolution of the Neo-Tethys, doi:10.5169/SEALS-166398.

Robertson, A., & P. Degnan (1994), The Dras arc Complex: Lithofacies and reconstruction of a Late Cretaceous oceanic volcanic arc in the Indus Suture Zone, Ladakh Himalaya, *Sedimentary Geology*, 92, 117–145.

Robin, P.-Y. F., & E. C. Jowett (1986), Computerized density contouring and statistical evaluation of orientation data using counting circles and continuous weighting functions, *Tectonophysics*, 121(2), 207–223, doi:10.1016/0040-1951(86)90044-2.

Robyr, M. (2002), Thrusting, Extension and Doming in the High Himalaya of Lahul Zanskar Area (NW India): Structural and Pressure-Temperature Constraints, vol. 40, 127–127 pp., Section des Sciences de la Terre, Université de Lausanne.

Robyr, M., & P. Lanari (2020), Kinematic, Metamorphic, and Age Constraints on the Miyar Thrust Zone: Implications for the Eohimalayan History of the High Himalayan Crystalline of NW India, *Tectonics*, 39(11), 1–24, doi:10.1029/2020TC006379.

Robyr, M., B. R. Hacker, & J. M. Mattinson (2006), Doming in compressional orogenic settings: New geochronological constraints from the NW Himalaya, *Tectonics*, 25(2), 1–19, doi:10.1029/2004TC001774.

Robyr, M., S. Banerjee, & A. El Korh (2012), Timing of prograde metamorphism in the High Himalaya of NW Lahul (NW India), *Journal of Nepal Geological Society*, 45, 101–102.

Robyr, M., J. L. Epard, & A. El Korh (2014), Structural, metamorphic and geochronological relations between the Zanskar Shear Zone and the Miyar Shear Zone (NW Indian Himalaya): Evidence for two distinct tectonic structures and implications for the evolution of the High Himalayan Crystalline of Zans, *Journal of Asian Earth Sciences*, 79(PA), 1–15, doi:10.1016/j.jseaes.2013.09.007.

Searle, M. P. (1983), Stratigraphy, structure and evolution of the Tibetan–Tethys zone in Zanskar and the Indus suture zone in the Ladakh Himalaya, *Transactions of the Royal Society of Edinburgh: Earth Sciences*, 73, 205–219, doi:10.1017/S0263593300009688.

Searle, M. P. (1986), Structural evolution and sequence of thrusting in the High Himalayan, Tibetan-Tethys and Indus suture zones of Zanskar and Ladakh, Western Himalaya, *Journal of Structural Geology*, 8(8), 923–936.

Searle, M. P., D. J. Waters, D. C. Rex, & R. N. Wilson (1992), Pressure, temperature and time constraints on Himalayan metamorphism from eastern Kashmir and western Zanskar, *Journal - Geological Society (London)*, 149(5), 753–773, doi:10.1144/gsjgs.149.5.0753.

Searle, M. P., D. J. Waters, M. W. Dransfield, B. J. Stephenson, C. B. Walker, J. D. Walker, & D. C. Rex (1999), Thermal and mechanical models for the structural and metamorphic

evolution of the Zanskar High Himalaya, *Geological Society, London, Special Publications*, 164(1), 139–156, doi:10.1144/GSL.SP.1999.164.01.08.

Shellnutt, J. G. (2018), The Panjal Traps, *Geological Society, London, Special Publications*, 463, 59–86, doi:10.1144/SP463.4.

Stäubli, A. (1989), Polyphase metamorphism and the development of the Main Central Thrust, *Journal of Metamorphic Geology*, 7, 73–93.

Stäubli, A. R. (1988), Metamorphose und Deformation im Bereich der zentralen Hauptüberschiebung (M.C.T.) (Kishtwar Fenster, NW-Himalaya), Ph.D. thesis, ETH Zurich.

Stephenson, B. J. (1997), The tectonic and metamorphic evolution of the Main Central Thrust zone and High Himalaya around the Kishtwar and Kulu windows, northwest India, Ph.D. thesis, University of Oxford.

Stephenson, B. J., D. J. Waters, & M. P. Searle (2000), Inverted metamorphism and the Main Central Thrust: Field relations and thermobarometric constraints from the Kishtwar Window, NW Indian Himalaya, *Journal of Metamorphic Geology*, 18(5), 571–590, doi: 10.1046/j.1525-1314.2000.00277.x.

Štípská, P., P. Závada, S. Collett, A. R. Kylander-Clark, B. R. Hacker, A. S. Tabaud, & M. Racek (2020), Eocene migmatite formation and diachronous burial revealed by petrochronology in NW Himalaya, Zanskar, *Journal of Metamorphic Geology*, 38(6), 655–691, doi:10.1111/JMG.12534.

Stübner, K., D. Grujic, R. R. Parrish, N. M. Roberts, A. Kronz, J. Wooden, & T. Ahmad (2014), Monazite geochronology unravels the timing of crustal thickening in NW Himalaya, *Lithos*, 210–211, 111–128, doi:10.1016/j.lithos.2014.09.024.

Thakur, S. S., & K. Tripathi (2008), Regional metamorphism in the Haimanta Group of rocks, Sutlej river valley, NW Himalaya, India, *Current Science*, 95(1), 104–109.

Thöni, M., C. Miller, C. Hager, B. Grasemann, & M. Horschinegg (2012), New geochronological constraints on the thermal and exhumation history of the Lesser and Higher Himalayan Crystalline Units in the Kullu-Kinnaur area of Himachal Pradesh (India), *Journal of Asian Earth Sciences*, 52, 98–116, doi:10.1016/j.jseaes.2012.02.015.

Vance, D., & N. Harris (1999), Timing of prograde metamorphism in the Zanskar Himalaya, *Geology*, 27(5), 395–398.

Vance, D., M. Ayres, S. Kelley, & N. Harris (1998), The thermal response of a metamorphic belt to extension: Constraints from laser Ar data on metamorphic micas, *Earth and Planetary Science Letters*, 162(1), 153–164, doi:10.1016/S0012-821X(98)00163-0.

Vannay, J.-C., & B. Grasemann (1998), Inverted metamorphism in the High Himalaya of Himachal (NW India) : Phase equilibria versus thermobarometry, *Schweizerische Mineralogische und Petrographische Mitteilungen*, 78(1), 107–132, doi:10.5169/SEALS-59277.

Vannay, J.-C., Z. D. Sharp, & B. Grasemann (1999), Himalayan inverted metamorphism constrained by oxygen isotope thermometry, *Contributions to Mineralogy and Petrology*, 137(1-2), 90–101, doi:10.1007/s004100050584.

Wadia, D. N. (1961), Geology of India, Macmillan, London.

Walker, C. B. (1999), The tectonothermal evolution of the High Himalaya in the Suru Valley, NW Zanskar with constraints from metamorphic modelling, Ph.D. thesis, University of Oxford.

Walker, C. B., M. P. Searle, & D. J. Waters (2001), An integrated tectonothermal model for the evolution of the high Himalaya in Western Zanskar with constraints from thermobarometry and metamorphic modeling, *Tectonics*, 20(6), 810–833, doi:10.1029/2000TC001249.

Walker, J. D., M. W. Martin, S. A. Bowring, M. P. Searle, D. J. Waters, & K. V. Hodges (1999), Metamorphism, Melting, and Extension: Age Constraints from the High Himalayan Slab of Southeast Zanskar and Northwest Lahaul, *The Journal of Geology*, 107(4), 473–495, doi:10.1086/314360.

Walsh, J., S. Buckman, & A. P. Nutman (2019), Age and Provenance of the Nindam Formation, Ladakh, NW Himalaya: Evolution of the Intraoceanic Dras Arc Before Collision With India, *Tectonics*, 38, 1–27, doi:10.1029/2019TC005494.

Wyss, M. (2000), Metamorphic evolution of the northern Himachal Himalaya: Phase equilibria constraints and thermobarometry, *Schweizerische mineralogische und petrographische Mitteilungen*, 80, 317–350, doi:10.5169/SEALS-60971.